PAPER

Check for updates

Selective formation of propan-1-ol from propylene *via* a chemical looping approach†

A. R. P. Harrison [iD] * and E. J. Marek [iD] *

A novel chemical looping approach for propan-1-ol production from propylene was investigated. Silver- and gold-based catalysts were prepared, with SrFeO$_{3-\delta}$ perovskite as a catalyst support, and characterised using X-ray diffraction (XRD), electron microscopy (SEM and STEM-EDS), and X-ray photoelectron spectroscopy (XPS). Particles of the catalysts were used in experiments carried out in a packed bed reactor, by passing 5 vol% propylene over the material to generate oxygenated products, with oxygen provided *via* reduction of the catalyst support, SrFeO$_{3-\delta}$. The solid particles were subsequently re-oxidised with air in a separate step, closing the chemical loop. Catalysts composed of AgCl and AgAu alloy supported on SrFeO$_{3-\delta}$ gave up to 70–80% stable selectivity towards propan-1-ol over the temperature range 260–300 °C, with little to no formation of the secondary alcohol, propan-2-ol, albeit at low propylene conversion (~0.5–1.5%). Postulated mechanisms for propan-1-ol formation under chemical looping conditions are discussed, *via* propylene oxide or allyl alcohol intermediates.

1. Introduction

Selective oxidation of propylene to form value-added C$_3$ products, such as propylene oxide (PO), allyl alcohol (AA), and propan-1-ol, is a significant challenge in heterogeneous catalysis.[1–4] In particular, catalysts for producing propylene oxide from propylene using air as the oxidising agent have been studied extensively,[5,6] but are not yet commercially competitive, despite the environmental and economic problems of the incumbent chlorohydrin and hydroperoxide processes.[1] Production of propan-1-ol directly from propylene is also challenging due to the preferential formation of the secondary alcohol isomer, propan-2-ol, under most reaction conditions.[4]

Silver-based catalysts on metal oxide supports have been widely investigated for selective oxidation of propylene,[6] but have generally shown relatively poor selectivity towards C$_3$ oxygenates. For propylene reacting with oxygen over Ag, the γ-carbon atom in propylene preferentially reacts with atoms of oxygen adsorbed at the Ag surface, O$_a$, to form CO$_2$ *via* complete combustion. The complete combustion reaction can be partially suppressed by the addition of chloride species, either on the surface of the catalyst or in the feed gas,[7–11] but at the penalty of decreased propylene conversion.

Selectivity towards C$_3$ oxygenates *via* oxidation of propylene is further limited by isomerisation reactions. Barteau and co-workers[12] investigated the reactions of PO

over Ag surfaces under aerobic and anaerobic conditions. They found that PO can undergo H-transfer reactions to form a broad distribution of products, including propanal, acetone, allyl alcohol, and acrolein.

The use of Ag–Au bimetallic catalysts in selective oxidation reactions has been investigated by Geenen *et al.*[13] Increasing the proportion of Au to Ag reduced the extent of complete combustion, with acrolein as the favoured oxygenate product. The increase in selectivity towards acrolein was attributed to the catalysts having isolated Ag sites (*i.e.* the separation between the catalyst's active sites greatly exceeded the size of propylene molecules), which inhibit the dissociation of molecular oxygen from forming two neighbouring O$_a$–Ag species. Therefore, the favoured surface species was adsorbed molecular (O$_2$)$_a$,[13,14] which is selective towards acrolein.

Previous studies have also investigated using solid oxides (*e.g.* PdO$_x$, VO$_x$) as oxidising agents for propylene oxidation.[15] Unsupported PdO$_x$ catalysts produced PO at up to 28% selectivity, with acrolein and propanal forming *via* isomerisation of PO at 38% and 33% selectivity, respectively. The overall conversion of propylene was low, at ~0.4%. However, the PdO$_x$ catalysts used did not show a consistent product distribution over multiple redox cycles, with ~98% selectivity towards acrolein at ~0.01% propylene conversion after regenerating the catalyst in air. The broad distribution of oxygenate products was ascribed to the ability of Pd to act as a catalyst for hydrogen transfer reactions, which aid isomerisation of PO to other oxygenates. In contrast, near 100% selectivity for PO was achieved using unsupported V$_2$O$_5$ as a solid oxidant, but at very low (~0.03%) conversion of propylene. The use of V$_2$O$_5$ supported on SiO$_2$ or γ-Al$_2$O$_3$

Department of Chemical Engineering and Biotechnology, University of Cambridge, Philippa Fawcett Drive, Cambridge, CB3 0AS, UK. E-mail: arph2@cam.ac.uk, ejm94@cam.ac.uk

2534 | *React. Chem. Eng.*, 2022, 7, 2534–2549

This journal is © The Royal Society of Chemistry 2022

allowed for a modest improvement in the conversion of propylene, up to ~0.1%, at ~70% selectivity towards PO over a single reduction step. The use of Bi_2O_3–MoO_3 and Fe_2SbO_x for oxidising propylene at elevated temperatures (>450 °C) has also been investigated.[16,17] Acrolein was found to be the dominant C_3 oxygenate product over the catalysts MoO_3, 2 $Bi_2O_3 \cdot MoO_3$, and Fe_2SbO_x, with C_6 hydrocarbons (benzene and hexadiene) being the favoured products over Bi_2O_3 and Sb_2O_4.

Recently, a chemical looping approach has been proposed[18] for selective oxidation reactions, including epoxidation of olefins,[19] oxidative dehydrogenation of alkanes,[20] or conversion of methane to methanol.[21] Here, lattice oxygen is provided from a metal oxide support (termed the oxygen carrier) to react at the surface of a catalyst, in the absence of gaseous oxygen. The oxygen carrier is then re-oxidised in air, in a separate step (a schematic of the process is shown in Fig. 1), giving the chemical looping approach the advantage of inherent separation between the organic species and the air, thereby decreasing the risk of forming explosive mixtures.

Studies on chemical looping for selective oxidation of ethylene[19,22,23] have used Ag deposited on a non-stoichiometric oxide, strontium ferrite, $SrFeO_{3-\delta}$, with perovskite structure, demonstrating chemical looping epoxidation of ethylene to ethylene oxide (EO). Strontium ferrite was chosen as a suitable oxygen carrier for selective oxidation reactions, as $SrFeO_{3-\delta}$ undergoes reversible oxygen release at relatively low temperatures (<300 °C),[19,24] and can be produced inexpensively *via* solid-state methods.[25]

The ratio of the perovskite phase, $SrFeO_3$, to Ruddlesden–Popper phase, $Sr_3Fe_2O_7$, was found to strongly influence the rate of release of oxygen from the $SrFeO_3$ support.[22] Catalysts for chemical looping epoxidation of ethylene have been found to give stable performance over 33 cycles,[23] producing EO at 67% selectivity, with 19% conversion of ethylene. Perovskite supports have also been investigated[26,27] for propylene epoxidation and found to improve modestly the selectivity towards PO, by facilitating the dissociation of O_2 molecules, but under conventional operating conditions with oxygen in the gas phase, rather than chemical looping.

In this work, Ag, AgCl, and Ag/Au catalysts, supported on $SrFeO_3$ perovskite, were investigated for chemical looping oxidation of propylene. Catalysts containing AgCl and/or Au

were found to give low levels of complete combustion, and high selectivity towards propan-1-ol. Interestingly, the AgCl and AgCl/Au catalysts produced a substantially different distribution of products as compared to typical distributions reported for direct epoxidation of propylene over Ag- and Au-based catalysts.[5] The results provide an insight into potential future challenges in applying a chemical looping approach to propylene oxidation, and indicate that catalysts composed of AgCl and, or AgAu alloy supported on $SrFeO_3$ may be suitable for production of propan-1-ol from propylene *via* a chemical looping approach.

2. Materials and methods

2.1. Material preparation

Active particles, composed of a metal catalyst supported on strontium ferrite, were prepared using various deposition methods. Strontium ferrite perovskite ($SrFeO_{3-\delta}$, written as $SrFeO_3$ for brevity) was prepared using a solid-state method.[25] Stoichiometric quantities of $SrCO_3$ (Sigma-Aldrich, 98%) and Fe_2O_3 (Fisher Scientific, 95%) were manually mixed to form a homogeneous powder; then, 50 mL ethanol (Sigma-Aldrich, >99.8%) was added as a binder. The mixture was milled in a planetary ball mill using ceramic balls placed with the mixture in a ceramic jar; ball-milling was carried out for 3 h at 25 Hz, then, the mixture was dried for 24 h at 50 °C. The resulting powder was sieved to 180–355 μm, 50–180 μm, and <50 μm size fractions, and calcined in air for 12 h at 1000 °C. Particles of $SrFeO_3$ were impregnated with metal catalysts using incipient wetness impregnation.

Preparation of Ag/SrFeO₃. To deposit Ag on $SrFeO_3$ particles, first, $AgNO_3$ (Alfa Aesar, >99.8%) was dissolved in DI water. The resulting solution was added dropwise to 2.00 g of $SrFeO_3$ (180–355 μm), followed by manual mixing with a spatula to ensure all liquid was absorbed. For the AgCl on $SrFeO_3$ catalyst, the addition of the $AgNO_3$ was followed by further introduction of 191 μL hydrochloric acid (37 wt%, VWR), again, added dropwise with manual mixing of the $SrFeO_3$ particles. The amount of acid introduced gave a 50 mol% excess of HCl with respect to Ag, ensuring that all Ag was able to react to form AgCl, with a target loading of 10 wt% AgCl with respect to $SrFeO_3$. Following the addition of the precursor solution, the material was dried at 120 °C for 12 h, then calcined at 650 °C for 5 h in static air.

Preparation of Au/SrFeO₃ and AgCl/Au/SrFeO₃. For catalyst samples containing gold, two preparation methods were used to impregnate Au particles onto $SrFeO_3$ supports. To impregnate $SrFeO_3$ with gold, a method adapted from Suo *et al.*[28] was used. Briefly, a batch of precursor solution containing gold was prepared by adding 0.486 g $AuCl_3$ (Alfa Aesar, >99.8%) to 0.752 mL DI water. The solution was adjusted to pH ~8 by introducing 0.355 mL NaOH solution (Fisher Scientific, 10% w/v), and afterwards, added dropwise to 2.00 g of $SrFeO_3$. Catalysts prepared by impregnation with $AuCl_3$ were designated Au-D/$SrFeO_3$.

A series of mixed AgCl/Au-D catalysts supported on $SrFeO_3$, with target metal loadings x wt% Ag and (10–x) wt% Au (x = 2.5, 5, 7.5), was prepared by varying the volume of Ag
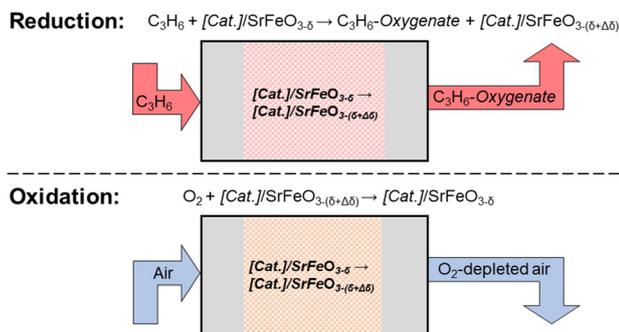

Fig. 1 Schematic diagram showing the reduction and oxidation steps in selective oxidation of propylene *via* chemical looping for a catalyst, Cat., supported on an oxygen carrier, here, strontium ferrite.

This journal is © The Royal Society of Chemistry 2022

React. Chem. Eng., 2022, **7**, 2534–2549 | **2535**

and Au solutions added (noting that $AgNO_3$ reacts with $AuCl_3$ in solution to form AgCl). The solutions of Ag and Au precursor were prepared separately, then added sequentially to the support material in appropriate ratios to achieve the desired loading, followed by overnight drying and calcination at 650 °C for 5 h. Catalysts prepared by impregnation with $AgNO_3$ and $AuCl_3$ were designated xAgCl/(10–x)Au-D/SrFeO$_3$.

One batch of this catalyst was also prepared by impregnating $SrFeO_3$ with $AgNO_3$ and $AgCl_3$ solutions, followed by drying at 120 °C and calcination at 700 °C for 5 h. Calcination at 700 °C as opposed to 650 °C induced thermal decomposition of AgCl,[29] giving a final loading of 3.4 wt% AgCl and a 5.1 wt% loading of Ag/AgAu. The sample calcined at 700 °C was designated Ag–AgCl/Au-H/SrFeO$_3$.

Preparation of Ag/Au-L/SrFeO$_3$. For chloride-free catalysts containing gold, a ligand complexation method from Murayama *et al.*[30] was used. Briefly, 1.82 mmol β-alanine (Acros Organics, 99%) was added to 2 mL NaOH solution (Fisher Scientific, 1.25 M), followed by adding 3 mL ethanol (Fisher Scientific, 99.8 vol%). A separate solution was prepared by adding 1 mL $HAuCl_4$ dissolved in DI water (Acros Organics, ACS Reagent; 0.227 M) to 4 mL ethanol. The two solutions were combined and cooled at −18 °C overnight, yielding a pale orange precipitate. The solids were collected *via* centrifugation at 528 RCF for 10 minutes at 4 °C, then washed with 70% v/v ethanol, and stored in a desiccator, obtaining Au–(β-ala). The dark Au–(β-ala) solid was then dissolved in 1.7 mL DI water, and 0.5 mL of the resultant solution was added dropwise to 2.00 g of $SrFeO_3$, with $AgNO_3$ solution sequentially added to produce a mixed Ag/Au catalyst. The sample was then dried at 120 °C for 12 h and calcined in air at 650 °C for 5 h. The catalyst prepared using Au–(β-ala) was designated Au-L. The resulting Au loading was determined by inductively coupled plasma atomic emission spectroscopy (ICP-AES) to be 0.02 wt%, the lowest of all gold-containing materials that were prepared here.

All samples investigated are summarised in Table 1.

2.2. Material characterisation

Powder X-ray diffraction (XRD) patterns were measured using a Bruker D8 Advance diffractometer, over the angular range

5–80° with step size 0.05° and step time 2 s, using Cu-Kα radiation. Phase composition was determined with Profex software,[31] using reference structures from the ICSD database[32] (collection codes are given in the ESI,† Table S1). Scanning electron microscopy (SEM) images were taken using a Tescan Mira3 FEG-SEM microscope with an accelerating voltage of 5 kV, and secondary electron (SE) and back-scattered electron (BSE) detectors in parallel. Scanning transmission electron microscopy (STEM) images were taken using a Thermo Scientific (FEI) Talos F200X G2 TEM with a SuperX energy-dispersive X-ray spectroscopy (EDS) detector.

X-ray photoelectron spectroscopy (XPS) measurements were taken using an Escalab 250Xi spectrometer, with 20 eV scan pass energy. Scans were calibrated with respect to the Au 4f$_{7/2}$ peak at 84.00 eV,[33] collected on an Au foil (Alfa Aesar, 99.9975+%). Samples of Ag foil (Alfa Aesar, 99.998%) and AgCl powder (Acros Organics, 99+%) were also scanned to determine the binding energy of 3d$_{5/2}$ for metallic Ag^0 and Ag$^+$. Collected results were deconvoluted to assess the electronic states for elements in the analysed samples. The analysis was performed using CasaXPS software.[34]

2.3. Experiments in a packed bed reactor

The performance of the prepared materials was determined using a small scale packed-bed reactor, operated in the chemical looping mode. A bed of active particles, composed of a metal catalyst impregnated on $SrFeO_3$ (1.50 g, 180–300 μm) was placed in a quartz tube, in between two layers of SiC (Alfa Aesar, 46 grit), with 2.00 g of SiC below and 3.00 g of SiC above the bed of active particles. A schematic of the experimental rig is given in the ESI,† Fig. S1. The bed was assembled in a quartz reactor tube (200 mm length, i.d. 8 mm), with a sintered disk supporting the bed 75 mm from the tube base. The reactor was secured using Swagelok Ultra-Torr vacuum fittings with fluorocarbon FKM O-rings, and wrapped with a heating tape (LewVac, 200 W). A K-type thermocouple, positioned in the centre of the active material, was used to control the setpoint temperature. The reactor was heated under air flow for 2 h prior to experiments, to ensure the setpoint temperature was achieved throughout the bed, and to remove carbonate and hydroxide species from the $SrFeO_3$ surface.[35] The gases used in experiments were 5 vol%

Table 1 Summary of catalyst samples used in chemical looping experiments, with a target total metal loading of 10 wt% for each sample. Catalyst loadings were estimated using X-ray diffraction (XRD) and ICP-AES measurements

Sample	Catalyst	Measured amount of catalyst, wt%	Catalyst precursors used	Heat treatment
Ag/SrFeO$_3$	Ag	11.8 wt% Ag	$AgNO_{3(aq)}$	120 °C for 12 h; 650 °C for 5 h
Au-D/SrFeO$_3$[a]	Au	7.3 wt% Au	Alkaline $AuCl_{3(aq)}$	120 °C for 12 h; 650 °C for 5 h
AgCl/SrFeO$_3$	AgCl	1.1 wt% Ag, 8.8 wt% AgCl	$AgNO_{3(aq)}$, treated with conc. $HCl_{(aq)}$	120 °C for 12 h; 650 °C for 5 h
xAgCl/(10–x)Au/SrFeO$_3$[a] (x = 2.5, 5, 7.5)	AgCl/Au	x = 2.5: 3.4 wt% AgCl, 7.9 wt% AgAu x = 5: 5.1 wt% AgCl, 5.1 wt% AgAu x = 7.5: 6.9 wt% AgCl, 5.1 wt% AgAu	$AgNO_{3(aq)}$, alkaline $AuCl_{3(aq)}$	120 °C for 12 h; 650 °C for 5 h
Ag–AgCl/Au-H/SrFeO$_3$[a]	Ag/AgCl/Au	3.4 wt% AgCl, 5.1 wt% (Ag + AgAu)	$AgNO_{3(aq)}$, alkaline $AuCl_{3(aq)}$	120 °C for 12 h; 700 °C for 5 h
Ag/Au-L/SrFeO$_3$[a]	Ag/Au	4.6 wt% Ag, 0.02 wt% Au	$AgNO_{3(aq)}$, Au–(β-ala)$_{(aq)}$	120 °C for 12 h; 650 °C for 5 h

[a] Letters in the sample codes stand for: D – impregnated with $AuCl_3$, H – impregnated with $AuCl_3$ followed by calcination at 700 °C to partially decompose AgCl, L – impregnated with chloride-free Au–(β-ala).

2536 | *React. Chem. Eng.*, 2022, **7**, 2534–2549

This journal is © The Royal Society of Chemistry 2022

$$X = \frac{\text{Total carbon in products (ppm)}}{\text{Total carbon detected (ppm)}} = \frac{[PO] + \frac{1}{3}[CO_2] + [\text{Propan-1-ol}] + [\text{Acetone}] + [\text{Propanal}] + [AA]}{[\text{Propylene}] + [PO] + \frac{1}{3}[CO_2] + [\text{Propan-1-ol}] + [\text{Acetone}] + [\text{Propanal}] + [AA]} \tag{1}$$

$$S_A = \frac{\text{Total carbon in A (ppm)}}{\text{Total carbon in products (ppm)}} = \frac{[A]}{[PO] + \frac{1}{3}[CO_2] + [\text{Propan-1-ol}] + [\text{Acetone}] + [\text{Propanal}] + [AA]} \tag{2}$$

$$O_{\text{release}} = F \int_0^{t_{\text{reduction}}} ([PO] + 3[CO_2] + [\text{Propan-1-ol}] + [\text{Acetone}] + [\text{Propanal}] + [AA]) dt \tag{3}$$

$$C_{\text{Balance}} = \frac{\text{Total carbon detected}}{\text{Total carbon in}} = \frac{[\text{Propylene}] + [PO] + \frac{1}{3}[CO_2] + [\text{Propan-1-ol}] + [\text{Acetone}] + [\text{Propanal}] + [AA]}{[\text{Propylene}]_{\text{Inlet}}} \tag{4}$$

propylene (balance Ar, BOC, 4.96 or 5.13 vol%) for reduction, N_2 (BOC) for purging, and air (BOC) for re-oxidation. Gas flows to the reactor were set to 200 mL min^{-1} (NTP). Reduction and oxidation cycles were performed by passing gases over the material in the sequence N_2–C_3H_6–N_2–air. Generally, in a single cycle, the active bed was reduced in C_3H_6 for 1.5 min, followed by a 2 min purge step in N_2, and then re-oxidised in air for 15 min. The effect of reduction time was also investigated, varying the reduction time from 1.5 min to 60 min, but keeping the 2 min purge in N_2 and 15 min reoxidation in air. The active bed was periodically regenerated by heating the packed reactor tube to 650 °C for 5 h *ex situ* in static air.

The gas from the reactor outlet was sampled manually using a gas syringe, withdrawing a 10 mL sample immediately after the reactor tube. Samples were collected 45 s after the start of each reduction step in C_3H_6/N_2. The gas composition was measured with an Agilent 7890A gas-chromatograph (GC), using parallel Agilent PoraBOND-Q and Hayesep-Q/MolSieve 13A columns, connected to FID and TCD detectors, respectively. The FID channel was used to quantify propylene, propylene oxide (PO), propanal, acetone, propan-1-ol, propan-2-ol, and allyl alcohol (AA), and the TCD channel was used to quantify CO_2. No CO, or other carbon-containing products, were detected above 5 ppm. The GC measurements were calibrated using two gas mixtures: (1) 1000 ppm propylene/1000 ppm propylene oxide/balance N_2; (2) 1000 ppm CO_2/balance N_2; both BOC. From measurements of calibration gas mixtures, the accuracy of the FID detection system was estimated to be within ±10% of the true value based on variability of results collected by measuring samples of known compositions. The detection threshold was 1–2 ppm for C_3 components containing oxygen. The accuracy of the TCD was estimated to be ±4% of the true value, with a detection threshold of 10 ppm CO_2. For other organic components, gas mixtures for calibration were generated using an Owlstone V-OVG vapour generator fed with pure liquid components (acetone: VWR, 99%; propan-1-ol: Sigma-Aldrich, 99+%; propan-2-ol, VWR, 99%; propanal: Acros Organics, 99+%; allyl alcohol: Sigma-Aldrich, 99+%). Retention times for each component were consistent to within ±0.05 min for all measurements.

Instantaneous conversion of propylene, X, was estimated from the concentrations measured at the reactor outlet, using (1).

Given the relatively low (<10%) conversion of propylene, the total molar flowrate was taken to be approximately constant before and after the reactor.

Selectivity towards a given product, S_A, (*i.e.* PO or propan-1-ol) was determined using (2).

Cumulative oxygen release was estimated using (3), where F is the molar flowrate of gas, $t_{\text{reduction}}$ is the reduction time, and with integrals estimated using the trapezium rule. The factor of 3 is applied to the CO_2 concentration to account for oxygen participating in the formation of CO_2 and H_2O during complete combustion, noting the 1:1 ratio of the two combustion products:

$$C_3H_6 + 4\frac{1}{2}O_2 \rightarrow 3CO_2 + 3H_2O. \tag{R1}$$
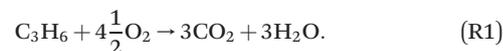
To confirm the validity of measurements, the carbon balance over each cycle was estimated using (4), where $[\text{Propylene}]_{\text{Inlet}}$ was taken to be equal to the concentration of propylene in the feed gas. For experiments using blended mixtures of gases, $[\text{Propylene}]_{\text{Inlet}}$ was determined using the GC. The overall carbon balance for all measurements was within ±10% of the expected value.

To determine potential side-reactions of oxidation products, chemical looping oxidation experiments were also performed using a propylene feed stream with PO or propanal added. An electrical tube furnace was used to heat the reactor tube as opposed to heating tape, with the active bed placed in the isothermal region of the furnace, using a rig previously described by Gebers *et al.*[23] An inlet gas mixture containing propylene and PO was produced by blending 5.13 vol% propylene (balance Ar) with 1000 ppm propylene/1000 ppm propylene oxide (balance N_2), using 100 mL min^{-1} of each mixture for a nominal composition of 2.56 vol% propylene and 500 ppm propylene oxide. In another experiment, an inlet gas mixture containing propylene and propanal was produced by passing 5.13 vol% propylene through a vapour generator (Owlstone, V-OVG) at 200 mL min^{-1}, loaded with propanal (Acros Organics, 99+%), thus, generating a stream containing 5.13 vol% propylene and ~1200 ppm propanal. The composition of gas mixtures blended in-house was confirmed with the GC. Similarly, a reaction of PO with hydrogen was investigated by blending 5

vol% H_2 (balance N_2; Air Liquide) with 1000 ppm propylene/1000 ppm propylene oxide (balance N_2), for a nominal composition of 500 ppm PO, 500 ppm propylene and 2.5 vol% H_2. The mixture of PO, propylene, and H_2 was then passed over the active bed, with the outlet stream composition measured using the GC.

3. Results

3.1. Material characterisation

Prepared catalysts were characterised with XRD and the results are presented in Fig. 2 and S3.† From the XRD patterns for $AgCl/SrFeO_3$, $AgCl/Au-D/SrFeO_3$ and $Ag–AgCl/Au-H/SrFeO_3$, peaks at $2\theta = 32.1°$ and $46.0°$ were detected, as shown in Fig. 2, corresponding to the AgCl crystalline phase. The characteristic peaks for AgCl were absent in the patterns for $Ag/SrFeO_3$ and $Ag/Au-L/SrFeO_3$. For the $AgCl/Au-D/SrFeO_3$ samples, no metallic Ag was detected, confirming AgCl and AgAu (alloyed Ag and Au) as the main phases containing silver.

The estimated compositions calculated for each sample are presented in Table S2.† The oxygen carrier was approximately pure $SrFeO_3$ (>95%). For the $Ag–AgCl/Au-H/SrFeO_3$ sample, calcined at 700 °C, Fig. 2 shows a less prominent AgCl peak than in the Au-D samples calcined at 650 °C, giving an AgCl loading of 3.4 wt% as compared to 5.1 wt%. The smaller AgCl peak confirms that calcination at 700 °C induced thermal decomposition of AgCl, which starts

around 650–700 °C.[29] No AgCl was detected in the sample prepared using the Au–(β-ala) precursor ($Ag/Au-L/SrFeO_3$), where all Ag and Au were present as metallic nanoparticles, with an Ag loading of 4.6 wt%. Given the close proximity of the Ag, Au, and AgAu XRD peaks, and the low Au loading (~0.02 wt%) determined from ICP measurements (Table 1), separate AgAu and Au peaks could not be refined for the $Ag/Au-L/SrFeO_3$ sample.

In Fig. S4,† XRD patterns for fresh, spent, and regenerated $AgCl/SrFeO_3$ are shown, with an AgCl fraction of ~10 wt% calculated for all three samples. The presence of AgCl in the spent sample indicates minimal stripping of chloride due to the reaction between propylene and AgCl, suggesting greater stability of bulk AgCl under reaction conditions as compared to Ag promoted with Cl^- ions at the surface.[10,11]

The presence of AgCl on the surface of the 5Ag/5Au-D/$SrFeO_3$ sample was confirmed *via* STEM-EDS surface mapping of crushed particles of supported catalysts, shown in Fig. 3 (further STEM-EDS maps are shown in Fig. S5 in the ESI†). Particles composed of AgCl and AgAu were detected on the surface, with AgAu forming larger particles and AgCl smaller (Sauter mean dia. of 266 nm and 111 nm, respectively). Low atomic fractions of Cl were detected in particles of AgAu, and low atomic fractions of Au in particles of AgCl (<5.0 at_{Cl}% and <0.6 at_{Au}%, respectively for all analysed particles), demonstrating limited overlap between AgAu and AgCl clusters. Analysis of the AgCl particles gave a molar ratio of Ag to Cl in
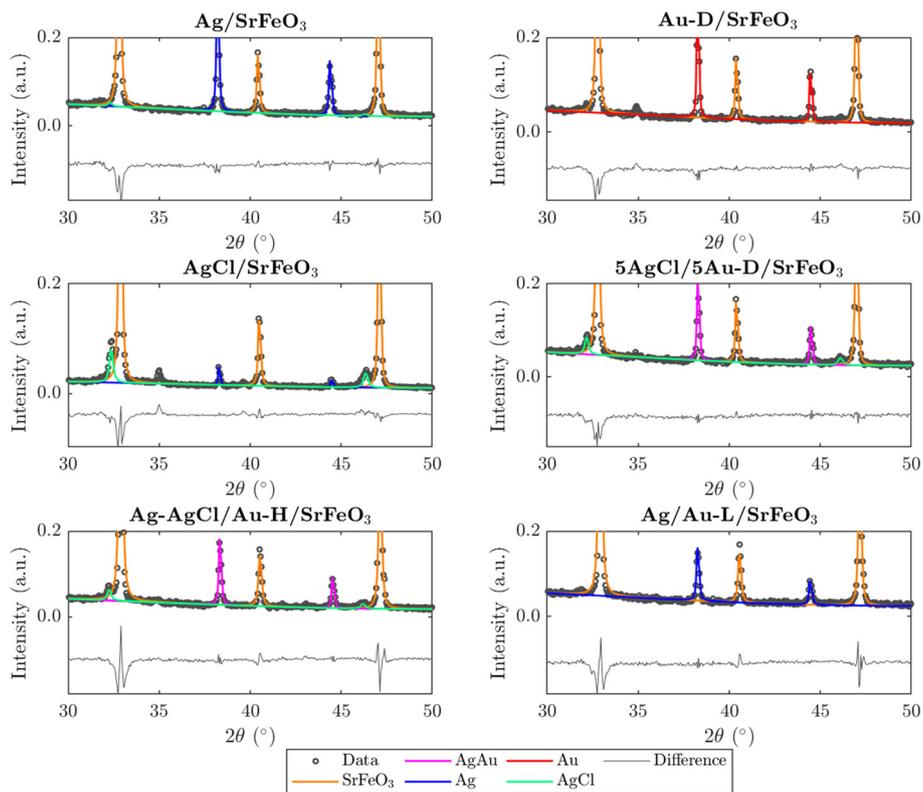

Fig. 2 Sections of collected XRD patterns for Ag/SrFeO₃, Au-D/SrFeO₃, AgCl/SrFeO₃, 5AgCl/5Au-D/SrFeO₃, Ag–AgCl/Au-H/SrFeO₃, and Ag/Au-L/SrFeO₃. Circles indicate experimental measurements; lines indicate fitted model using reference patterns.

2538 | *React. Chem. Eng.*, 2022, **7**, 2534–2549

This journal is © The Royal Society of Chemistry 2022

the range ~1–2 with an Ag : Cl ratio of 1 corresponding to pure AgCl, and an Ag : Cl ratio of 2 corresponding to 50 at% AgCl and 50 at% Ag. Thus, Ag was present either as particles of AgCl or clusters of metallic Ag with AgCl. For areas of bare $SrFeO_3$ support, no Ag or Au was detected, and the Sr : Fe atomic ratio was close to 1 in all cases.

The surface of the catalyst particles was further characterised using SEM images (shown in the ESI,† Fig. S6 and S7). Notably, from Fig. S7† for $5Ag/5Au-D/SrFeO_3$, two distinct surface particle morphologies were observed, with larger (~425 nm), approximately spherical particles, and smaller (~135 nm), elongated particles visible (particle size distributions are given in the ESI,† Fig. S8). Additionally, the larger particles appeared brighter in the BSE image, corresponding to greater atomic number,[36] which indicates the mixture of AgAu, as compared to the smaller, darker particles, composed of AgCl.

The surface states of the elements in the supported catalysts were determined by XPS, with the full analysis described in the ESI,† section S5. The XPS spectra for the $5Ag/5Au-D/SrFeO_3$ sample, presented in Fig. 4a and b, demonstrate shifts in binding energy for Ag 3d and Au 4f in AgAu, thus, indicating an alloying behaviour between the two metals, with the extent of the shifts in agreement with values reported in literature.[37–40] Only two distinct peaks were detected in the O 1s spectra for $5AgCl/5Au-D/SrFeO_3$ and $AgCl/SrFeO_3$. The oxygen feature at a lower binding energy of 528.3–530.4 eV (shown in red in Fig. 4c) was assigned to lattice oxygen in $SrFeO_3$,[41] while the feature at a higher binding energy of 530.8–533.8 eV (shown in blue in Fig. 4c) was assigned to carbonate or hydroxide species adsorbed at

the surface of the $SrFeO_3$.[41,42] Additionally, the XPS spectra recorded for the O 1s peak suggest the presence of small amounts of AgO_x species at the surface of $Ag/SrFeO_3$ (assigned at 529.5 eV, shown in green in Fig. 4c) that were not detected for any of the other catalyst samples. In Fig. 4d, the AgCl standard and $AgCl/SrFeO_3$ samples show the Cl $2p_{3/2}$ peak at 198.8 eV, and $2p_{3/2}–2p_{1/2}$ peak separation of $c.$ 1.6 eV, in good agreement with literature.[43] A peak shift of −1.5 eV between the $2p_{3/2}$ AgCl standard and the $AgCl/SrFeO_3$ sample was observed, which is similar to the shift reported for thin layers (~5 nm) of AgCl in contact with Ag.[43,44]

3.2. Performance in chemical looping experiments

Results from experiments carried out in the packed bed for $5AgCl/5Au-D/SrFeO_3$ catalysts are presented in Fig. 5. The catalysts showed considerable activity towards propan-1-ol formation, with outlet concentrations of ~100–500 ppm propan-1-ol, a product not detected in previous studies of propylene oxidation over AgCl or Au catalysts[8,10,11,13,14] Trace amounts of PO, acetone, propanal, and propan-2-ol (~5 ppm) were also measured. Over five cycles of reduction and re-oxidation, the outlet concentrations of propan-1-ol and CO_2 remained approximately stable, indicating minimal catalyst deactivation with cycling. For the sample of $5Ag/5Au-D/SrFeO_3$, increasing the reactor temperature from 260 °C to 300 °C resulted in greater overall conversion of propylene, from ~0.5 to ~1.5%, but with limited effect on selectivity towards propan-1-ol, which remained at 60 ± 4% over the temperature range. The approximately constant selectivity with temperature is surprising; seemingly, the apparent rates of the formation of propan-1-ol and of complete combustion have similar temperature dependence over the range 260 °C to 300 °C, and hence, the ratio of propan-1-ol to CO_2 in the reaction products does not change significantly.

The effect of altering flowrate of the propylene feed ($F_{C_3H_6}$) to the bed of 5Ag/5Au-D/SFO catalyst was also investigated; results are shown in Fig. S13.† The obtained trends are similar to those in Fig. 5 when increasing the temperature, namely, a longer residence time ($0.5F_{C_3H_6}$) resulted in the improved conversion of C_3H_6. For that case, the selectivity to propan-1-ol dropped to ~42%. When the residence time decreased ($2F_{C_3H_6}$), the selectivity remained similar to that at $1F_{C_3H_6}$, namely, ~60%. This minimal change in selectivity with temperature and residence time of propylene gives evidence that competing parallel and, or consecutive reactions are at play. Possible reactions that lead to the formation of propan-1-ol are further discussed in section 4.2.

Longer reduction steps (120 min) were performed over two $AgCl/Au-D/SrFeO_3$ catalysts (Fig. S10†), showing total oxygen release greater than the oxygen available from Ag_2O or from oxygen adsorbed at the catalyst surface (calculations for O are given in the ESI,† section S7, eqn (S2)–(S4)). For the more active sample ($7.5AgCl/2.5Au-D/SrFeO_3$), the rate of oxygen release decreased with time as expected when oxygen for reaction is sourced from a solid oxygen carrier,[45] here,

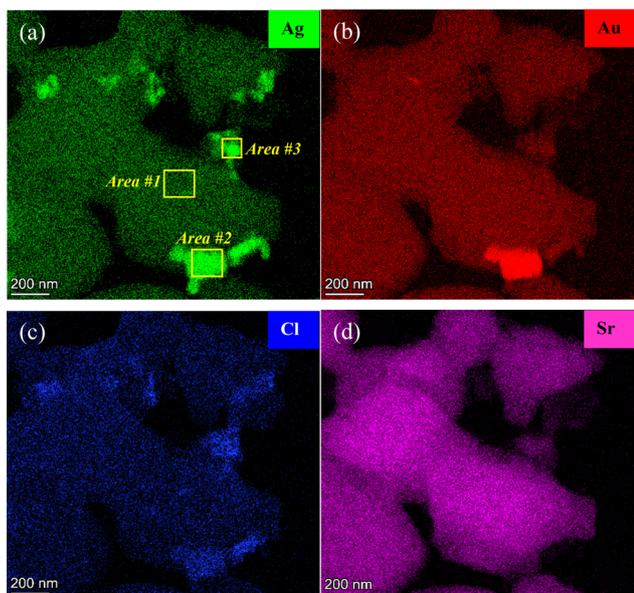**Fig. 3** STEM-EDS maps of crushed $5Ag/5Au-D/SrFeO_3$ particles, showing distribution of (a) Ag, (b) Au, (c) Cl, (d) Sr. Area 1 corresponds to bare $SrFeO_3$ support with no Ag or Au detected, Area 2 corresponds to a particle of AgAu, Area 3 corresponds to a particle of AgCl.

This journal is © The Royal Society of Chemistry 2022

React. Chem. Eng., 2022, **7**, 2534–2549 | **2539**
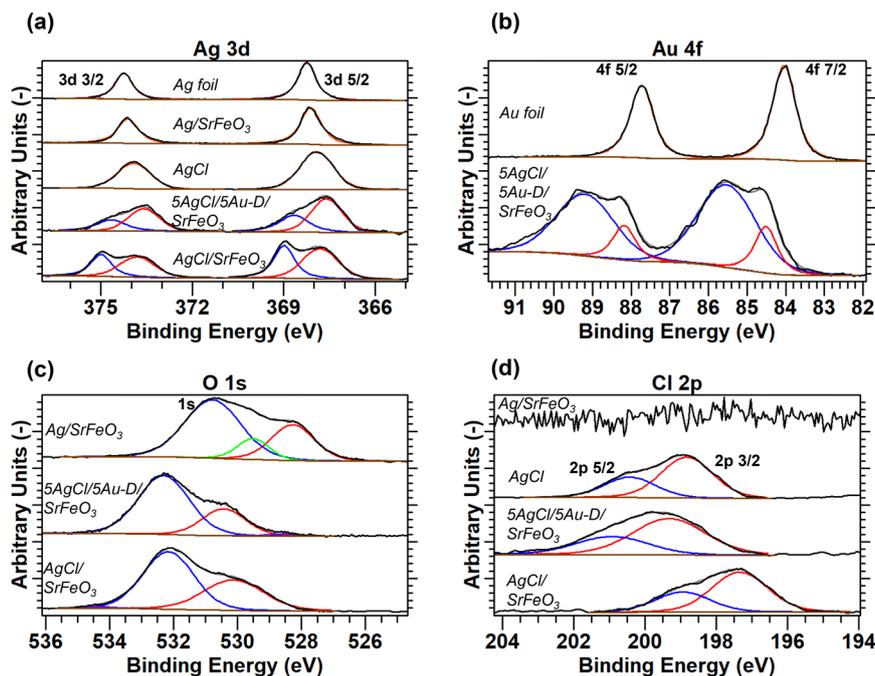
Fig. 4 XPS spectra for (a) Ag 3d, (b) Au 4f, (c) Cl 2p, and (d) O 1s scans, with deconvoluted peaks fitted to experimental measurements. Measurements calibrated with respect to Au $4f_{7/2}$ peak at BE = 84.0 eV. Full details of peak deconvolution are given in the ESI,† Table S4.
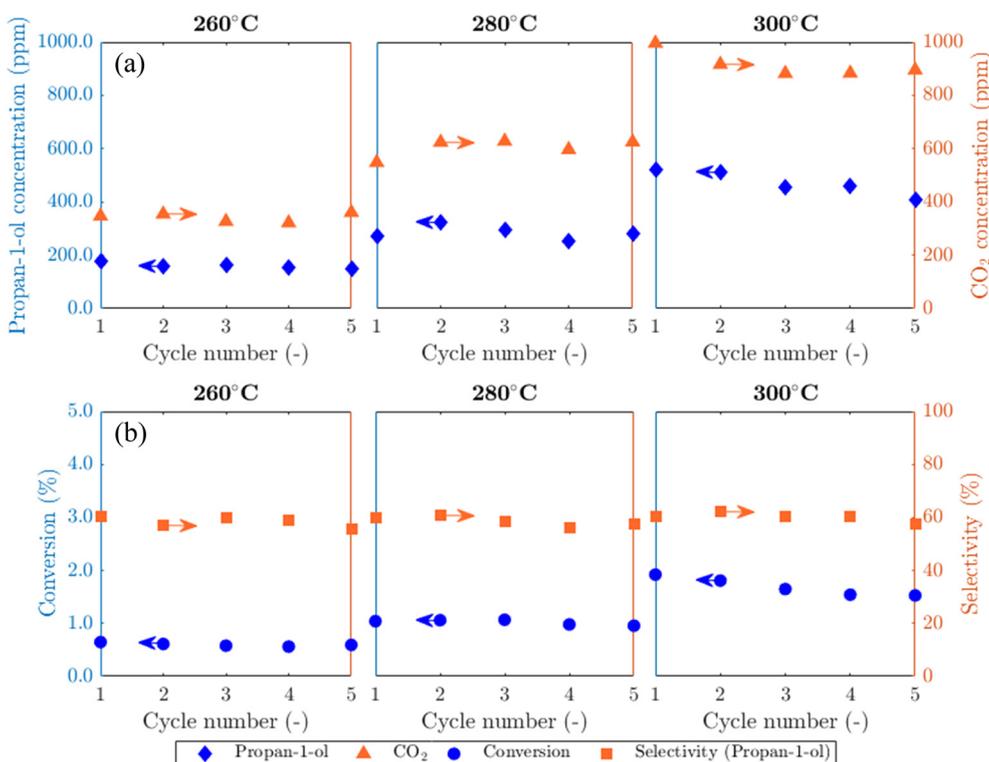
Fig. 5 (a) Concentrations of propan-1-ol and CO_2 and (b) calculated propylene conversion and selectivity towards propan-1-ol (shown on left and right axes, respectively) over the temperature range 260–300 °C for 5AgCl/5Au-D/SrFeO$_3$.

SrFeO$_3$. Given that the overall propylene conversion in the standard cycling experiments (Fig. 5a) was low, a reduction time of longer than 1.5 min may be achievable without

impacting the catalytic performance, as the amount of oxygen accumulated in the gaseous products after 1.5 min of reduction corresponds to a very small change in SrFeO$_{3-\delta}$

stoichiometry ($\Delta\delta \ll 0.01$). To determine the feasibility of increasing the length of the reduction step in chemical looping, redox cycling was performed over 7.5AgCl/2.5Au-D/SrFeO$_3$, with the duration of the reduction step increased each cycle, as presented in Fig. 6. Fig. 6b shows that conversion of propylene rapidly decreases with reduction time up to ~8–9 min reduction, but later declines slowly. The observed behaviour can be modelled as the sum of two exponential decay functions, given in Fig. 6b. This therefore suggests that the rate limiting step may change over the course of extended reduction, potentially from kinetic limitation by the surface reaction, to mass-transfer limitation from oxygen diffusing from bulk SrFeO$_3$ to the catalyst surface. Selectivity to propan-1-ol remains ~40% if reduction is shorter than 10 min, as shown in Fig. 6c. Decrease in performance with prolonged reduction has been previously observed for chemical looping epoxidation of ethylene[19,23] and, to some degree, associated with the decreasing availability of oxygen from SrFeO$_3$.

The effect of altering the Ag to Au ratio in xAgCl/(10–x)Au/SrFeO$_3$ catalysts was investigated, with average values of conversion of propylene and selectivity towards propan-1-ol and PO shown in Fig. 7, where error bars indicate the standard deviation taken from 5 redox cycles. Increasing the Ag loading in the Ag–Au mix at the catalyst surface increased the overall conversion of propylene, but the change was primarily driven by complete combustion rather than selective oxidation to desired products (outlet concentrations for each component are given in the ESI,† Fig. S9). Therefore, combustion of propylene likely occurs on Ag sites, as previously reported in studies of propylene oxidation with gaseous oxygen.[5] Additionally, for all

catalyst compositions, higher temperatures resulted in an increase in total conversion of propylene, but again, with unclear and only little effect on selectivity to propan-1-ol.

Selectivity towards propan-1-ol reached a maximum of ~80% for the sample with a loading of 2.5AgCl/7.5Au-D/SrFeO$_3$, with the selectivity decreasing with higher total Ag loading. The highest propan-1-ol concentration of ~470 ppm in the outlet stream was observed in experiments with the 7.5AgCl/2.5Au-D/SrFeO$_3$ sample (presented in Fig. S9†) at 300 °C. However, the result was accompanied by a high concentration of CO$_2$, giving a lower overall selectivity for propan-1-ol than the sample of 2.5AgCl/7.5Au-D/SrFeO$_3$.

For PO, the oxygenate product detected with second-highest concentration (Fig. 7), altering the loading of Ag and Au in the AgCl/Au-D/SrFeO$_3$ samples had only limited effect on selectivity. For samples where appreciable concentrations of PO (up to 20 ppm, in Fig. S9†) were detected at the reactor outlet, namely Au-D/SrFeO$_3$ and 7.5AgCl/2.5Au-D/SrFeO$_3$, selectivities towards PO remained low, regardless of the operating temperatures, primarily, because the main products were still CO$_2$ and propan-1-ol.

Results comparing the performance of Ag/SrFeO$_3$ and AgCl/SrFeO$_3$ are shown in Fig. 8. For the Ag/SrFeO$_3$ sample, a notable decrease in catalyst activity was observed after the first chemical looping cycle, with PO concentration decreasing to near-zero, and CO$_2$ concentration more than halving for all cycles. Contrastingly, the AgCl/SrFeO$_3$ sample showed comparatively stable performance over 5 cycles, with substantially greater propan-1-ol concentrations than observed with the Ag/SrFeO$_3$ samples, and lower concentrations of CO$_2$. All cycles over AgCl/SrFeO$_3$ gave low
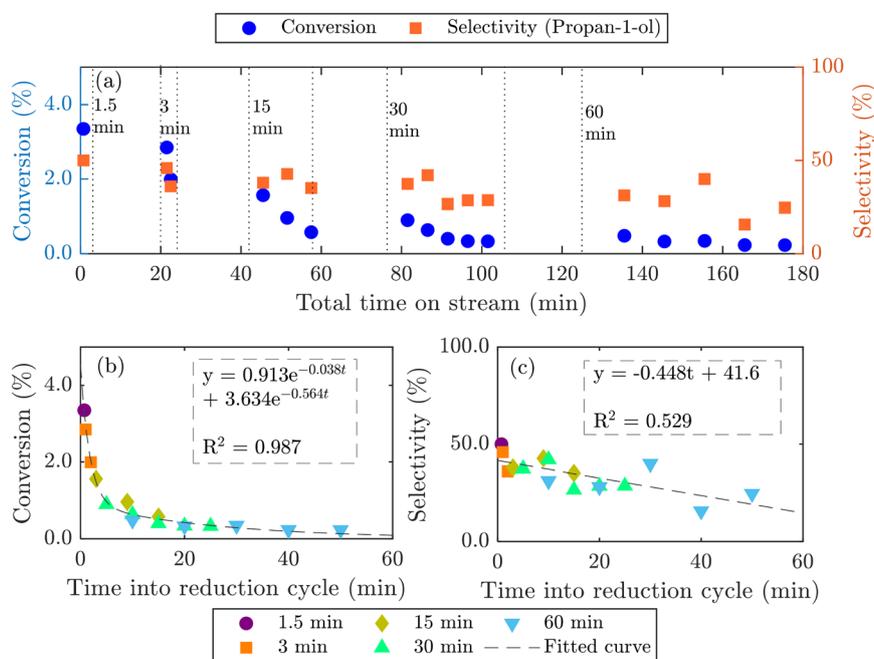

Fig. 6 Chemical looping over 7.5AgCl/2.5Au-D/SrFeO$_3$, with reduction time increased from 1.5 to 60 min. Vertical dotted lines in (a) indicate start and end of each reduction step. Change in conversion of propylene (b), and in selectivity towards propan-1-ol (c).
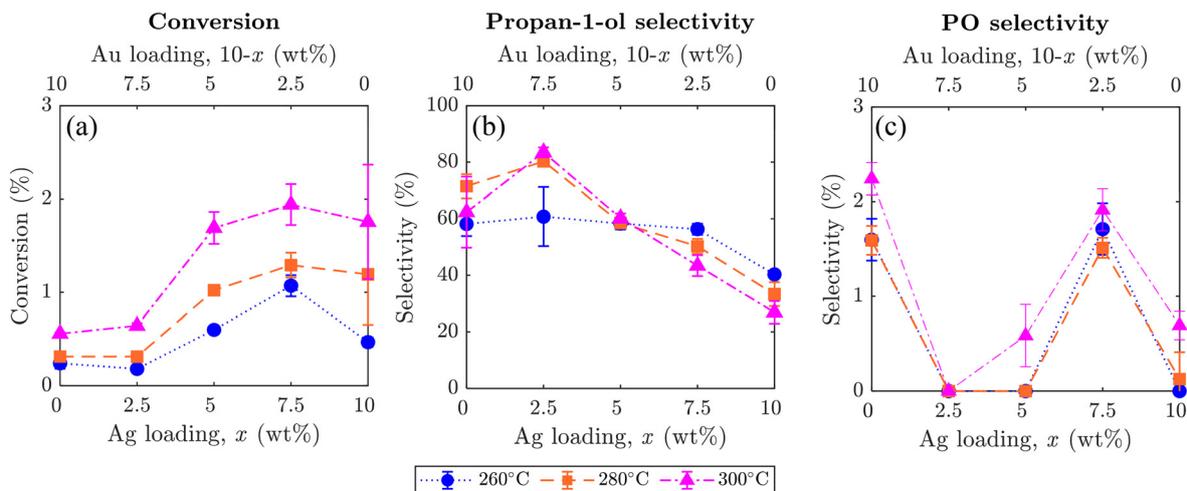
Fig. 7 Graphs showing average values of (a) propylene conversion, (b) selectivity towards propan-1-ol, and (c) selectivity towards PO, for xAgCl/$(10-x)$Au-D/SrFeO$_3$ samples ($x = 0$, 2.5, 5, 7.5, 10). Error bars show standard deviation over 5 cycles, noting that some error bars are smaller than the datapoint markers. Sample at $x = 0$ corresponds to Au-D/SrFeO$_3$; sample at $x = 10$ corresponds to AgCl/SrFeO$_3$.

concentrations of PO at the outlet, below 6.0 ppm. The rapid decrease in PO formation over Ag/SrFeO$_3$ after the first cycle suggests that PO was formed via reaction with AgO$_x$ surface species, as detected by XPS. As Ag$_2$O and AgO are not thermodynamically stable at 260 °C or above,[46] the silver oxides would not be regenerated during the oxidation step of chemical looping.

No AgO$_x$ species were detected at the surface of AgCl/SrFeO$_3$ from XPS measurements, which may explain the lower levels of PO. For both catalysts, raising the temperature from 260 °C to 300 °C resulted in an increase in overall conversion, primarily driven by combustion. Interestingly, however, increasing temperature with Ag/SrFeO$_3$ did not result in a significant change in outlet propan-1-ol concentrations.

The effect of changing the preparation method for Au-containing catalysts was also investigated. In Fig. 9a and b, the product distributions of 5Ag/5Au-D/SrFeO$_3$ (calcined at 650 °C), Ag–AgCl/Au-H/SrFeO$_3$ (calcined at 700 °C to induce

thermal decomposition of AgCl), and Ag/Au-L/SrFeO$_3$ (prepared using Au–(β-ala) precursor) are compared.

Under chemical looping conditions at 280 °C, the Ag–AgCl/Au-H/SrFeO$_3$ sample produced a 65% greater concentration of propan-1-ol than the 5AgCl/5Au-D/SrFeO$_3$ sample, with an average outlet concentration of 470 ppm propan-1-ol (Fig. 9 and S11†). However, concentration of CO$_2$ was also ~60% higher. Propanal, allyl alcohol, and propylene oxide, were detected at low levels (10–20 ppm) for the Ag–AgCl/Au-H/SrFeO$_3$ sample, whereas none were detected for the 5AgCl/5Au-D/SrFeO$_3$.

For the chloride-free Ag/Au-L/SrFeO$_3$ sample containing only small amount of Au (0.02 wt%), a substantially different product distribution was measured as compared to the samples containing AgCl. The highest concentrations of PO (~70 ppm) were detected in the outlet stream for Ag/Au-L/SrFeO$_3$ as well as a slight decrease in propan-1-ol concentration as compared to 5AgCl/5Au-D/SrFeO$_3$ or Ag–AgCl/Au-H/SrFeO$_3$. However, the
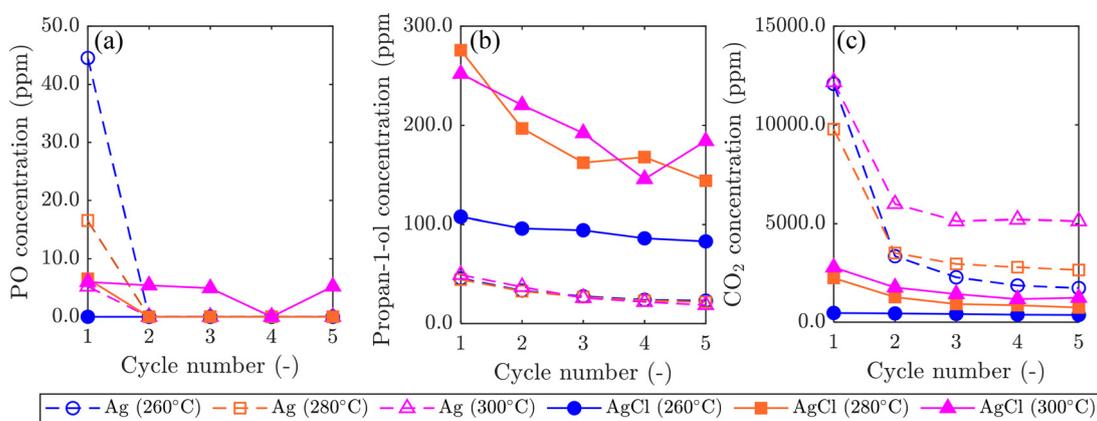

Fig. 8 Graphs showing comparison of reaction products: (a) PO, (b) propan-1-ol, and (c) CO$_2$ in experiments over Ag/SrFeO$_3$ and AgCl/SrFeO$_3$, in the temperature range 260–300 °C. Lines between cycles included to help differentiate samples.
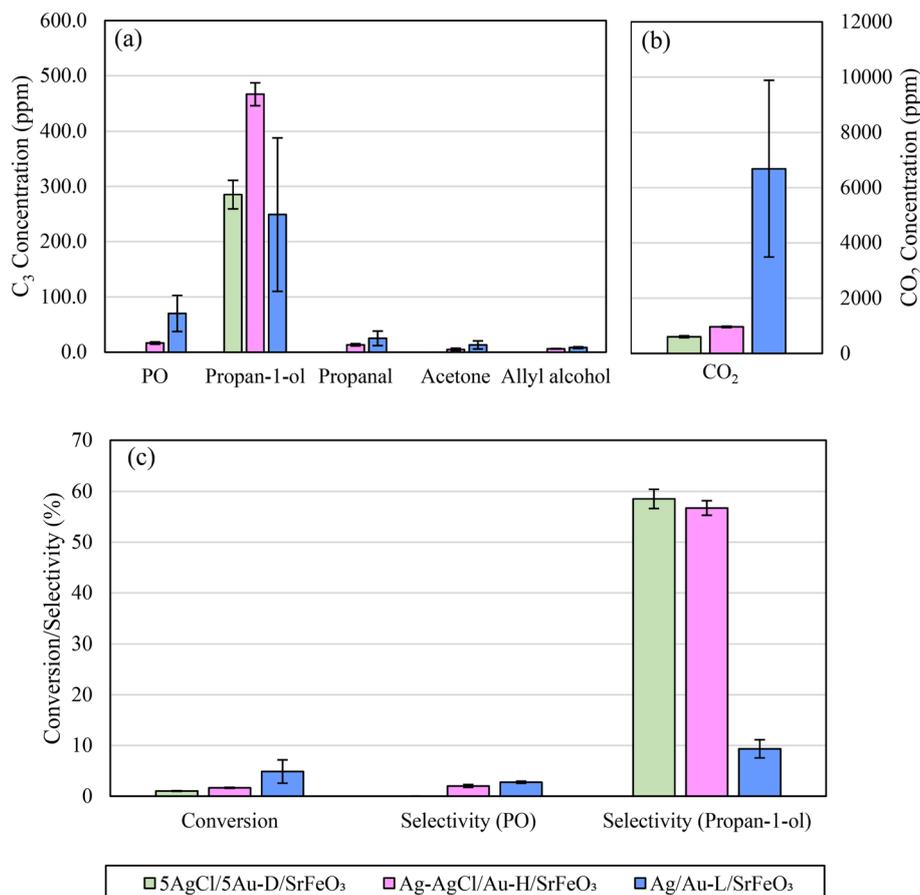
Fig. 9 Comparison of (a) concentrations of C_3 products, (b) concentrations of CO_2, and (c) overall conversion and selectivity, for 5AgCl/5Au-D/SrFeO₃, Ag–AgCl/Au-H/SrFeO₃, and Ag/Au-L/SrFeO₃ at 280 °C. Error bars correspond to standard deviation over 5 cycles.

selectivity towards C_3 oxygenates was markedly lower, due to a substantial increase in complete combustion. Average concentrations of CO_2 detected were an order of magnitude greater than for other samples containing gold and were comparable with Ag/SrFeO₃. Furthermore, for the Ag/Au-L/SrFeO₃ sample, a substantial decrease in activity was measured over the course of 6 cycles (shown in Fig. S12†), in a manner similar to the Ag/SrFeO₃ sample. We conclude that the presence of gold, even in minimal quantities (here, 0.02 wt%) was essential for producing PO, but that the overall behaviour of the Ag/Au-L/SrFeO₃ catalyst was dictated by the dominant metal, Ag.

4. Discussion

4.1. Effect of Cl and Au on product distribution

In this study, AgCl catalysts were found to favour selective oxidation of propylene, whereas metallic Ag favoured complete combustion, both when comparing Ag/SrFeO₃ and AgCl/SrFeO₃ (Fig. 8), and when considering 5AgCl/5Au-D/SrFeO₃ vs. Ag–AgCl/Au-H/SrFeO₃ and Ag/Au-L/SrFeO₃ catalysts (Fig. 9). In previous studies with gaseous oxygen, unsupported bulk AgCl was found to be essentially inert with respect to oxidation of propylene,[8,9] although a three-phase mixture of Ag, AgCl and CuO was demonstrated to be

somewhat selective towards formation of propylene oxide.[9] Furthermore, Ag catalysts promoted with ~5 wt% NaCl to form mixed Ag–AgCl catalysts, both without supports[7,8] and with non-reactive metal oxide supports,[11] have shown appreciable conversion and selectivity towards propylene oxide and acrolein. The lack of activity over AgCl alone is potentially due to strong adsorption of molecular oxygen at the surface of AgCl with limited $O_{2(g)}$ dissociation,[47] as compared to favourable dissociation of O_2 over Ag (ref. 47) to form reactive O_a–Ag sites.

The finding that the addition of Cl inhibits complete combustion, but enhances selective oxidation, is in line with previous investigations into the effect of Cl on propylene oxidation,[7,8,10,11,48] however, previous studies focused on small amount of Cl for promoting selective reactions. In studies on direct epoxidation of propylene with $O_{2(g)}$,[8] promotion of Ag catalysts NaCl to form a mixed Ag–AgCl catalyst substantially reduced the overall conversion of propylene, accompanied by an approximately proportional increase in selectivity towards propylene oxide. The presence of Cl⁻ was found to suppress total oxidation of propylene by making adsorbed oxygen more electrophilic.[8] The fact that, here, the AgCl-containing catalysts were found to be active towards formation of both propan-1-ol and CO_2, may be

This journal is © The Royal Society of Chemistry 2022

React. Chem. Eng., 2022, 7, 2534–2549 | **2543**

because oxygen is provided from the lattice of the oxygen carrier, $SrFeO_3$, as dissociated O atoms. Additionally, bulk AgCl has been demonstrated to be capable of accommodating and transporting oxygen, for example, Jayaraman and Yang used AgCl as a sorbent for pressure-swing adsorption of oxygen,[49] demonstrating its notable adsorption capacity, and relatively rapid oxygen transport through the AgCl structure. Similarly, the results here demonstrate that AgCl on $SrFeO_3$ can provide reactive atomic O_a species also to catalytic reactions. Comparison of oxygen adsorption and dissolution on AgCl, Ag, and Au is provided in the ESI,† section S7.

For the Ag/Au-L/$SrFeO_3$ sample, the gold loading was found to be low (~0.02 wt%), and as such the Au likely acted as a promoter for the Ag catalyst, rather than forming bulk AgAu alloy, although the exact mechanism remains unclear. The presence of Au strongly affected the process selectivity, with Ag/Au-L/$SrFeO_3$ catalyst producing the highest concentration of PO, and limited propan-1-ol (as shown in Fig. 9). An order of magnitude more CO_2 was detected for reaction over the Ag/Au-L/$SrFeO_3$ catalyst as compared to 5AgCl/5Au-D/$SrFeO_3$ and Ag–AgCl/Au-H/$SrFeO_3$, which was expected to take place on the metallic Ag surface present in Ag/Au-L/$SrFeO_3$. The increase in CO_2 for the chloride-free sample also supports the hypothesis that Cl species suppress complete combustion.

Given that both AgCl/$SrFeO_3$ and Au-D/$SrFeO_3$ showed appreciable selectivity towards propan-1-ol, both AgCl and Au must be catalytically selective in the chemical looping arrangement towards propan-1-ol. From Fig. 7b, maximum selectivity towards propan-1-ol was observed for the sample of 2.5AgCl/7.5Au/$SrFeO_3$, where both catalysts (AgCl and Au) were present. However, STEM-EDS images (Fig. 3) show little overlap between AgCl and AgAu particles, thus, possible synergy is unclear. Furthermore, from SEM and STEM-EDS (presented in Fig. 3 and S6–S8†), AgCl is present as relatively small particles (~100 nm), which are likely to be catalytically active, whereas AgAu is present as larger chunks (~400 nm). For AgAu, the reaction likely occurred at atomic-scale Ag sites at the surface of the large AgAu particles, as demonstrated in previous studies.[13,14]

The increase in propylene conversion with increasing ratio of Ag to Au on $SrFeO_3$ (as shown in Fig. 7a) suggests a faster rate of reaction at nanoparticles of AgCl catalyst than at nanoparticles of AgAu alloy catalyst. An extended reduction cycle (shown in Fig. S10†) also indicated a markedly faster rate of total release of oxygen in reactions over 7.5AgCl/2.5Au-D/$SrFeO_3$ as compared to 2.5AgCl/7.5Au-D/$SrFeO_3$. For the latter material, the rate of oxygen release was approximately constant over 100 min, suggesting that the process was limited by surface reactions between propylene and O_a species. In contrast, for the particles of 7.5AgCl/2.5Au-D/$SrFeO_3$, rate of oxygen release decreased over 100 min. Reduction times that are substantially longer than 1.5 min may be feasible over the catalysts investigated, however, chemical looping over 7.5AgCl/2.5Au-D/$SrFeO_3$ showed that conversion rapidly decreases for reduction times up to 8–9 min before levelling off (shown in

Fig. 7), and that selectivity gradually declines with longer reduction steps. Results presented in Fig. 5, however, confirm that chemical looping with 1.5 min (*i.e.* where regeneration of the oxygen carrier is more frequent) leads to stable selectivity across at least 5 cycles.

4.2. Mechanisms for propan-1-ol formation

In this work, a different product distribution was detected as compared to any other studies reported in literature[5,6] for propylene oxidation over Ag/Au catalysts, with propan-1-ol as a major reaction product. While the main difference is the delivery of oxygen to reactions (here, from $SrFeO_3$, while in other studies from the gas feed), the reason for the selective formation of propan-1-ol rather than any other possible oxygenates is unclear. Thus, we analysed several potential mechanisms for formation of the primary C_3 alcohol, starting with direct hydration of propylene by H_2O.[50] Given that in all experiments complete combustion occurred, water vapour was expected to be present in the reaction mixture. However, a hydration mechanism of propylene would predict formation of both primary and secondary alcohols, with propan-2-ol being the favoured product, because of the stabilisation of the secondary carbocation intermediate *via* electronic induction from the two methyl groups on either side of the localised positive charge.[4,50] Given that <5 ppm of propan-2-ol was detected as compared to up to 500 ppm propan-1-ol under chemical looping conditions, the direct hydration mechanism appears unlikely. Furthermore, addition of 2700 ppm H_2O to propylene during reduction did not result in a significant change in outlet propan-1-ol concentration (shown in ESI,† Fig. S18), suggesting that reaction between propylene and water is unlikely.

Another possible mechanism considered involves an oxygenated intermediate: PO, which forms and reacts further *via* the following reactions:

$$C_3H_6 + O \rightarrow C_3H_6O$$
$$C_3H_6O + 2H \rightarrow C_3H_7OH \tag{R2}$$
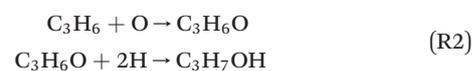
For the second step in (R2), a list of possible reactions of PO with hydrogen to form other C_3 oxygenates were considered, as summarised in Fig. 10a.

The mechanisms shown in Fig. 10a involving a C_3 oxygenate intermediate reacting with hydrogen to form propan-1-ol clearly require the presence of hydrogen in the reaction stream. A potential source of hydrogen in the chemical looping setup could originate from propylene coking at the catalyst surface. With no oxygen present in the gas-phase during the step when the hydrocarbon is oxidised, any hydrogen formed may be able to go on to react with oxygenate intermediates to form propan-1-ol, or with lattice oxygen to form water. However, in the experiments presented, no hydrogen was detected in the outlet stream. Another possibility is that hydrogen may be supplied from water or surface hydroxide species absorbed on the $SrFeO_3$ surface, which were also possibly detected *via* XPS (Fig. 4). Moreover, the addition of excess gaseous hydrogen to the

2544 | *React. Chem. Eng.*, 2022, **7**, 2534–2549

This journal is © The Royal Society of Chemistry 2022

Fig. 10 (a) Summary of main reactions of PO reported in literature. * = ref. 12, † = ref. 51 and 52, § = ref. 53 and 54, ¤ = ref. 55 and 56, ‡ = ref. 57 and 58. (b) Linear and branched oxametallacycle (OMC) surface species.[12,54]

propylene feed stream during the reduction step resulted in the preferential reaction of H_2 with surface O_a species, or with the $SrFeO_3$ oxygen carrier, to form water, limiting the oxygen available for reaction with C_3 species (shown in ESI,† Fig. S19).

Reactions between propylene oxide and H_2 have been investigated over various metal catalysts. Bartók and co-workers found that for propylene oxide, reaction over strongly electrophilic Ni or Cu catalysts resulted in the splitting of the more sterically hindered C–O bond in the PO molecule, forming a linear oxametallacycle species (Fig. 10b), which then reacts with H_2 and subsequently desorbs to form propan-1-ol or propanal (shown in Fig. 10a, green solid lines).[53,54] In contrast, when PO with H_2 was passed over less electrophilic catalysts, such as Pt or Pd, splitting of the less sterically hindered C–O bond was favoured, forming a branched oxametallacycle species. The branched surface species, presented in Fig. 10b, could then react with H_2, and desorb forming propan-2-ol or acetone. As AgCl is highly electrophilic,[8] it may behave similarly to the Ni or Cu surfaces when exposed to PO. Therefore, propan-1-ol may form over xAgCl/(10−x)Au-D/$SrFeO_3$ catalysts by initial formation of PO, followed by the reaction of the PO with H_2 at a strongly electrophilic AgCl surface. Gold and gold–silver surfaces might be expected to behave in a similar manner to Pt or Pd, *i.e.* by forming a non-electrophilic surface. The Au surface would then be expected to favour formation of branched oxametallacycle surface species and, consequently, secondary oxygenate products (acetone and

propan-2-ol). However, Au-D/$SrFeO_3$ was primary active towards propan-1-ol oxygenate (shown in Fig. 7), with little to no selectivity towards acetone or propan-2-ol, suggesting electrophilic behaviour and linear oxametallacycle route. The electrophilic behaviour of Au agrees with the finding[59] that noble metals impregnated on perovskites transfer electrons to the perovskite oxide on top of which there are deposited, resulting in an electrophilic metal surface.

For reactions over Ag/$SrFeO_3$ (Fig. 8), although Ag surfaces are able to facilitate the formation of OMC species[12] resulting in trace concentrations of propan-1-ol, the primary reaction product was CO_2, due to catalytic combustion of propylene *via* allylic hydrogen stripping.[5]

To determine whether the mechanism of propan-1-ol formation *via* hydrogenation of PO is plausible, chemical looping experiments were performed with PO added to the feed stream. Fig. 11a presents the measured compositions of the feed gas at the inlet of the packed-bed reactor and after the bed of 5Ag/5Au-D/$SrFeO_3$. For comparison, the gas mixture in one of the experiments contained only propylene (nominal concentration ~3 vol%), while in the other, contained propylene and PO (~3 vol% and 400 ppm, respectively).

When passing 2.5 vol% propylene over 5AgCl/5Au-D/$SrFeO_3$ with PO in the gas feed, significantly less propan-1-ol was formed, and more CO_2. When lower concentrations (500 ppm) of propylene and PO were fed over the bed of 5Ag/5Au-

This journal is © The Royal Society of Chemistry 2022

React. Chem. Eng., 2022, **7**, 2534–2549 | **2545**

D/SrFeO$_3$ particles, as shown in Fig. 11b, propan-1-ol was not detected in the outlet, with acetone and propanal being the only C3 oxygenate products above 5 ppm. The situation did not change after including H$_2$ in the feed, for an experiment with a 'PO:propylene:H$_2$' mixture. However, the additional PO from the feed may compete with propylene for adsorption sites, and once adsorbed, become fully oxidised to CO$_2$, rather than being hydrogenated to form propan-1-ol. Therefore, hydrogenation of PO to form propan-1-ol appears to be feasible only prior to the oxametallacycle desorbing.

Barteau and co-workers[12] proposed that for PO adsorbed onto an Ag surface, the gaseous PO, and linear and branched oxametallacycle intermediates are in equilibrium. Therefore, any PO added to the inlet stream would increase the amount of all intermediates that can isomerise to propan-1-ol but also other C$_3$ oxygenates. They also suggested that the linear oxametallacycle is able to undergo a linear 1,2 hydrogen shift, and then desorb as allyl alcohol (shown in Fig. 10a, blue dashed lines). Under aerobic conditions with O$_{2(g)}$, any allyl alcohol formed was found to rapidly become dehydrogenated to form acrolein, which then fully oxidised to CO$_2$. Low levels (6–10 ppm) of allyl alcohol were detected

in the outlet stream for reaction of propylene over Ag–AgCl/Au-H/SrFeO$_3$ and Ag/Au-L/SrFeO$_3$ samples (shown in Fig. 9a). Allyl alcohol that is adsorbed on Ag is also able to react with adsorbed hydrogen, H$_a$, to form propan-1-ol (Fig. 10a, pink dash-dotted lines).[51,52] Therefore, allyl alcohol may form by reaction of propylene with O$_a$ without rapidly dehydrogenating to acrolein, and then undergo hydrogenation at the catalyst surface to form propan-1-ol.

Reactions between PO and allyl alcohol, and propanal and allyl alcohol, have been reported by Imanaka and co-workers.[57,58] A hydrogen transfer reaction between one molecule of PO or propanal and one molecule of allyl alcohol occurs, to form propan-1-ol and acrolein in a 1:1 molar ratio (Fig. 10a, brown dotted lines). Reaction between PO and allyl alcohol may occur over AgCl/Au/SrFeO$_3$ catalysts; however, the hydrogen transfer reaction would predict acrolein forming in a 1:1 ratio with propan-1-ol. As no acrolein was detected in the chemical looping experiments, the reaction between PO and allyl alcohol is unlikely to contribute significantly to overall propan-1-ol formation reported here. Furthermore, propanal was predicted to also undergo reaction with allyl alcohol to form propan-1-ol and acrolein.[58]
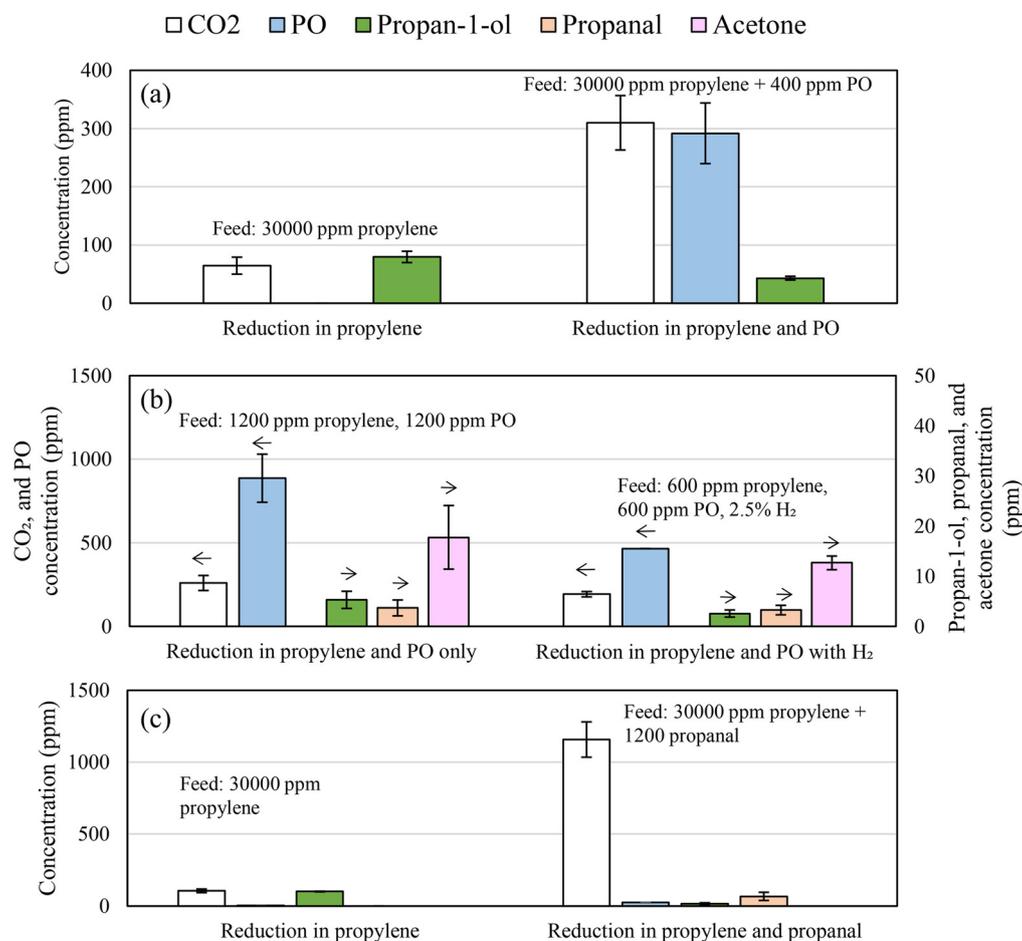

Fig. 11 Reaction products for reaction over 5Ag/5Au-D/SrFeO$_3$, for (a) propylene with and without PO added (b) dilute PO/propylene, with and without H$_2$ (c) for propylene with and without propanal added. Error bars show standard deviation from 3 cycles, arrows indicate y-axis for each species. Feed composition given on each figure, with balance gas Ar/N$_2$.

Given that adding propanal to the experimental feed stream (shown in Fig. 11c) resulted in a moderate decrease in propan-1-ol formation, the reaction between allyl alcohol and propanal is also discounted as a major source of propan-1-ol in the outlet stream.

The reaction of aldehydes and ketones (*i.e.* propanal and acetone) with hydrogen over gold catalysts to form primary or secondary alcohols, respectively, has been investigated *via* TPD studies by Pan and co-workers.[55,56] The authors found that in the case of hydrogen atoms adsorbed on Au(111), hydrogenation of propanal to propan-1-ol was favoured, and that minimal hydrogenation of acetone to propan-2-ol occurs, as the reaction pathway to form propan-2-ol is not thermodynamically favourable. Hydrogenation of propanal to propan-1-ol would be consistent with the observed experimental results that propan-1-ol is produced in substantially greater quantities over the mixed AgCl/Au catalysts, as opposed to Au alone. To determine if propan-1-ol formation *via* propanal was feasible, ~1200 ppm propanal was added to the 5 vol% propylene feed stream over 5AgCl/5Au-D/SrFeO$_3$ catalyst. Fig. 11c shows that the addition of propanal to the inlet feed did not increase the concentration of propan-1-ol measured in the outlet, and instead, showed an increase in complete combustion only. The lack of an increase in propan-1-ol concentration suggests that any propanal formed over AgCl/Au-D/SrFeO$_3$ catalysts undergoes further oxidation to CO$_2$, and so that the reaction mechanism for propan-1-ol formation is unlikely to proceed *via* propanal.

In summary, the most likely reaction mechanism for propan-1-ol formation is concluded to proceed *via* initial reaction of propylene with adsorbed surface O$_a$ to form a linear oxametallacycle surface species. The linear oxametallacycle then either reacts directly with hydrogen to form propan-1-ol, or undergoes a hydrogen shift to form allyl alcohol, which is subsequently hydrogenated to propan-1-ol. Further understanding of the surface mechanism may be achieved by performing density-functional theory (DFT) calculations of the hypothesised transition states, or through surface-sensitive experimental measurements (*e.g. in situ* XPS measurements of Ag and Au surface states over chemical looping cycles).

5. Conclusions

The selective oxidation of propylene *via* a chemical looping approach was demonstrated with AgCl, AgAu and mixed AgCl/Au catalysts supported on SrFeO$_3$ showing considerable selectivity towards propan-1-ol, with limited formation of other oxygenates. Catalysts containing AgCl were more selective to propan-1-ol as compared to Ag, which promoted complete combustion. Performance of the AgCl/Au catalysts was sensitive to the ratio of Ag and Au, with higher Ag content leading to favoured combustion over any oxygenated products. Selectivity towards propan-1-ol reaching 80% was achieved over 2.5AgCl/7.5Au-D/SrFeO$_3$ catalyst, albeit at <1%

propylene conversion. In contrast, Ag/Au-L/SrFeO$_3$, led to PO as a major C$_3$ product. Both results demonstrate that chemical looping can lead to new reaction pathways, strongly depended on the oxygen carrier and the catalyst. The mechanism of the chemical looping formation of propan-1-ol was also discussed, showing that the most likely pathway proceeds by surface reactions of oxametallacycle intermediates, rather than desorption and subsequent reabsorption of oxygenated species.

Author contributions

ARPH: material synthesis and characterisation, experiments, formal analysis, methodology, writing—original draft, revision. EJM: supervision, conceptualisation, writing—original draft, revision, funding acquisition. All authors read and approved the final manuscript.

Conflicts of interest

The authors have no competing interests to declare that are relevant to the article content.

Acknowledgements

References

1 D. L. Trent, *Kirk-Othmer Encycl. Chem. Technol.*, 2000, DOI: **10.1002/0471238961.1618151620180514.a01**.

2 D. Arntz, A. Fischer, M. Höpp, S. Jacobi, J. Sauer, T. Ohara, T. Sato, N. Shimizu and H. Schwind, *Ullmann's Encycl. Ind. Chem.*, 2007, DOI: **10.1002/14356007.a01_149.pub2**.

3 M. McCoy, *Chem. Eng. News Arch.*, 2001, **79**, 19–20.

4 J. Li, Z. Qin, H. Xu, M. Dong, J. Dong and J. Wang, *Ind. Eng. Chem. Res.*, 2007, **46**, 9000–9005.

5 S. J. Khatib and S. T. Oyama, *Catal. Rev.: Sci. Eng.*, 2015, **57**, 306–344.

6 J. Teržan, M. Huš, B. Likozar and P. Djinović, *ACS Catal.*, 2020, **10**, 13415–13436.

7 G. Lu and X. Zuo, *Catal. Lett.*, 1999, **58**, 67–70.

This journal is © The Royal Society of Chemistry 2022

React. Chem. Eng., 2022, **7**, 2534–2549 | **2547**

8 J. Lu, M. Luo, H. Lei and C. Li, *Appl. Catal., A*, 2002, **237**, 11–19.

9 M. Luo, J. Lu and C. Li, *Catal. Lett.*, 2003, **86**, 43–49.

10 A. Seubsai and S. Senkan, *ChemCatChem*, 2011, **3**, 1751–1754.

11 I. D. Charisteidis and K. S. Triantafyllidis, *Catal. Today*, 2020, **355**, 654–664.

12 A. Kulkarni, M. Bedolla-Pantoja, S. Singh, R. F. Lobo, M. Mavrikakis and M. A. Barteau, *Top. Catal.*, 2012, **55**, 3–12.

13 P. Geenen, H. Boss and G. Pott, *J. Catal.*, 1982, **77**, 499–510.

14 S. Rojluechai, S. Chavadej, J. W. Schwank and V. Meeyoo, *Catal. Commun.*, 2007, **8**, 57–64.

15 A. Dibenedetto, M. Aresta, C. Fragale, M. Distaso, C. Pastore, A. Venezia, C. Liu and M. Zhang, *Catal. Today*, 2008, **137**, 44–51.

16 V. Fattore, Z. Fuhrman, G. Manara and B. Notari, *J. Catal.*, 1975, **37**, 215–222.

17 V. Fattore, Z. Fuhrman, G. Manara and B. Notari, *J. Catal.*, 1975, **37**, 223–231.

18 X. Zhu, Q. Imtiaz, F. Donat, C. R. Müller and F. Li, *Energy Environ. Sci.*, 2020, **13**, 772–804.

19 M. S. C. Chan, E. Marek, S. A. Scott and J. S. Dennis, *J. Catal.*, 2018, **359**, 1–7.

20 Y. Gao, L. M. Neal and F. Li, *ACS Catal.*, 2016, **6**, 7293–7302.

21 T. Sheppard, C. D. Hamill, A. Goguet, D. W. Rooney and J. M. Thompson, *Chem. Commun.*, 2014, **50**, 11053–11055.

22 S. Gabra, E. J. Marek, S. Poulston, G. Williams and J. S. Dennis, *Appl. Catal., B*, 2021, **286**, 119821.

23 J. C. Gebers, A. R. P. Harrison and E. J. Marek, *Discov. Chem. Eng.*, 2022, **2**, 4.

24 C. Y. Lau, M. T. Dunstan, W. Hu, C. P. Grey and S. A. Scott, *Energy Environ. Sci.*, 2017, **10**, 818–831.

25 E. Marek, W. Hu, M. Gaultois, C. P. Grey and S. A. Scott, *Appl. Energy*, 2018, **223**, 369–382.

26 J. Lei, J. Dai, K. B. Tan, J. Huang, G. Zhan and Q. Li, *ACS Sustainable Chem. Eng.*, 2021, **9**, 794–808.

27 X. Zhang, J. Dai, J. Ding, K. B. Tan, G. Zhan, J. Huang and Q. Li, *Catal. Sci. Technol.*, 2022, **12**, 2426–2437.

28 Z. Suo, M. Jin, J. Lu, Z. Wei and C. Li, *J. Nat. Gas Chem.*, 2008, **17**, 184–190.

29 M. R. H. Siddiqui, S. F. Adil, M. E. Assal, R. Ali and A. A. Al-Warthan, *Asian J. Chem.*, 2013, **25**, 3405–3409.

30 H. Murayama, T. Hasegawa, Y. Yamamoto, M. Tone, M. Kimura, T. Ishida, T. Honma, M. Okumura, A. Isogai, T. Fujii and M. Tokunaga, *J. Catal.*, 2017, **353**, 74–80.

31 N. Doebelin and R. Kleeberg, *J. Appl. Crystallogr.*, 2015, **48**, 1573–1580.

32 A. Belsky, M. Hellenbrandt, V. L. Karen and P. Luksch, *Acta Crystallogr., Sect. B: Struct. Sci.*, 2002, **58**, 364–369.

33 M. P. Seah, I. S. Gilmore and G. Beamson, *Surf. Interface Anal.*, 1998, **26**, 642–649.

34 N. Fairley, V. Fernandez, M. Richard-Plouet, C. Guillot-Deudon, J. Walton, E. Smith, D. Flahaut, M. Greiner, M. Biesinger, S. Tougaard, D. Morgan and J. Baltrusaitis, *Appl. Surf. Sci. Adv.*, 2021, **5**, 100112.

35 E. J. Marek and E. García-Calvo Conde, *Chem. Eng. J.*, 2020, **417**, 127981.

36 G. E. Lloyd, *Mineral. Mag.*, 1987, **51**, 3–19.

37 N. N. Kariuki, J. Luo, M. M. Maye, S. A. Hassan, T. Menard, H. R. Naslund, Y. Lin, C. Wang, M. H. Engelhard and C.-J. Zhong, *Langmuir*, 2004, **20**, 11240–11246.

38 S. Malathi, T. Ezhilarasu, T. Abiraman and S. Balasubramanian, *Carbohydr. Polym.*, 2014, **111**, 734–743.

39 I. Srnová-Šloufová, B. Vlčková, Z. Bastl and T. L. Hasslett, *Langmuir*, 2004, **20**, 3407–3415.

40 R. J. Chimentão, I. Cota, A. Dafinov, F. Medina, J. E. Sueiras, J. L. G. de la Fuente, J. L. G. Fierro, Y. Cesteros and P. Salagre, *J. Mater. Res.*, 2006, **21**, 105–111.

41 H. Falcón, J. A. Barbero, J. A. Alonso, M. J. Martínez-Lope and J. L. G. Fierro, *Chem. Mater.*, 2002, **14**, 2325–2333.

42 A. Abd El-Naser, E. K. Abdel-Khalek, E. Nabhan, D. A. Rayan, M. S. Gaafar and N. S. Abd El-Aal, *Philos. Mag.*, 2020, **101**, 710–728.

43 V. K. Kaushik, *J. Electron Spectrosc. Relat. Phenom.*, 1991, **56**, 273–277.

44 Y. Qin, Y. Cui, Z. Tian, Y. Wu and Y. Li, *Nanoscale Res. Lett.*, 2017, **12**, 247.

45 B. Bulfin, J. Vieten, S. Richter, J. M. Naik, G. R. Patzke, M. Roeb, C. Sattler and A. Steinfeld, *Phys. Chem. Chem. Phys.*, 2020, **22**, 2466–2474.

46 I. Karakaya and W. T. Thompson, *J. Phase Equilib.*, 1992, **13**, 137–142.

47 S. Kim, S.-C. Lee, C. Lee, M. H. Kim and Y. Lee, *Nano Energy*, 2018, **48**, 134–143.

48 J. Lu, J. J. Bravo-Suárez, M. Haruta and S. T. Oyama, *Appl. Catal., A*, 2006, **302**, 283–295.

49 A. Jayaraman and R. T. Yang, *Chem. Eng. Sci.*, 2005, **60**, 625–634.

50 J. E. Logsdon and R. A. Loke, *Kirk-Othmer Encycl. Chem. Technol.*, 2000, DOI: **10.1002/0471238961.0919151612150719. a01**.

51 K. Brandt, M. E. Chiu, D. J. Watson, M. S. Tikhov and R. M. Lambert, *J. Am. Chem. Soc.*, 2009, **131**, 17286–17290.

52 M. Bron, D. Teschner, A. Knopgericke, B. Steinhauer, A. Scheybal, M. Havecker, D. Wang, R. Fodisch, D. Honicke and A. Wootsche, *J. Catal.*, 2005, **234**, 37–47.

53 F. Notheisz, Á. Molnár, Á. Zsigmond and M. Bartók, *J. Catal.*, 1986, **98**, 131–137.

54 M. Bartók, F. Notheisz and Á. Zsigmond, *J. Catal.*, 1980, **63**, 364–371.

55 M. Pan, Z. D. Pozun, A. J. Brush, G. Henkelman and C. B. Mullins, *ChemCatChem*, 2012, **4**, 1241–1244.

2548 | *React. Chem. Eng.*, 2022, **7**, 2534–2549

This journal is © The Royal Society of Chemistry 2022

56 M. Pan, A. J. Brush, Z. D. Pozun, H. C. Ham, W.-Y. Yu, G. Henkelman, G. S. Hwang and C. B. Mullins, *Chem. Soc. Rev.*, 2013, **42**, 5002.

57 T. Imanaka, Y. Okamoto and S. Teranishi, *Bull. Chem. Soc. Jpn.*, 1972, **45**, 1353–1357.

58 Y. Okamoto, T. Imanaka and S. Teranishi, *Bull. Chem. Soc. Jpn.*, 1973, **46**, 4–8.

59 Q. Wang, Y. Gu, W. Zhu, L. Han, F. Pan and C. Song, *Adv. Funct. Mater.*, 2021, **31**, 1–9.

This journal is © The Royal Society of Chemistry 2022

React. Chem. Eng., 2022, **7**, 2534–2549 | **2549**